Article:
Xu, S, Xu, J, Liu, Y-Z et al. (5 more authors) (2019) Constructing Mono-/Di-/Tri-Types of Active Sites in MoS2 Film toward Understanding Their Electrocatalytic Activity for the Hydrogen Evolution. ACS Applied Energy Materials, 2 (12). pp. 8974-8984. ISSN 2574-0962

https://doi.org/10.1021/acsaem.9b02084

Constructing Mono-/Di-/Tri-Types of Active Sites in MoS_2 Film toward Understand Their Electrocatalytic Activity for the Hydrogen Evolution

Journal:	*ACS Applied Energy Materials*
Manuscript ID	ae-2019-020843.R2
Manuscript Type:	Article
Date Submitted by the Author:	n/a
Complete List of Authors:	Xu, Shusheng; University of Leeds, Institute of Functional Surfaces, School of Mechanical Engineering Xu, Jiao; Chinese Academy of Sciences, State Key Laboratory of Solid Lubrication, Lanzhou Institute of Chemical Physics; Southern University of Science and Technology, School of Material Science and Engineering Liu, Yu-Zhen; Yonsei University, Centre for Nano-Wear, School of Mechanical Engineering Hua, Yong; University of Leeds, Institute of Functional Surfaces, School of Mechanical Engineering Duan, Zewen; Chinese Academy of Sciences, State Key Laboratory of Solid Lubrication, Lanzhou Institute of Chemical Physics Wang, Yanan; Chinese Academy of Sciences, State Key Laboratory of Solid Lubrication, Lanzhou Institute of Chemical Physics Neville, Anne; University of Leeds, School of Mechanical Engineering Gao, Xiaoming; Chinese Academy of Sciences, State Key Laboratory of Solid Lubrication, Lanzhou Institute of Chemical Physics

Constructing Mono-/Di-/Tri-Types of Active Sites in MoS_2 Film toward Understand Their Electrocatalytic Activity for the Hydrogen Evolution

Shusheng Xu[†,#], Jiao Xu[‡,§,#], Yu-Zhen Liu[‖], Yong Hua[†], Zewen Duan[‡], Yanan Wang[‡,*], Anne Neville[†,*], Xiaoming Gao[‡]

[†] *Institute of Functional Surfaces, School of Mechanical Engineering, University of Leeds, Leeds, LS2 9JT, UK*

[‡] *State Key Laboratory of Solid Lubrication, Lanzhou Institute of Chemical Physics, Chinese Academy of Sciences, Lanzhou 730000, People's Republic of China*

[§] *School of Material Science and Engineering, Southern University of Science and Technology, Shenzhen 518055, People's Republic of China*

[‖] *Centre for Nano-Wear, School of Mechanical Engineering, Yonsei University, Seoul 03722, Republic of Korea*

ABSTRACT

The availability and catalytic activity of the cost-efficient electrocatalysts are the dominant factors for the hydrogen evolution reaction (HER) performance in the renewable hydrogen economy. Extensive efforts have been devoted to maximize the amount of various active sites in non-noble metal electrocatalysts for HER. This work reported a physically-sputtering strategy to construct porous and ordered 2*H*-MoS_2 films with mono-/di-/tri-types of active sites *via* controlling the film thickness (from ~15 nm to 3050 nm) in the energetic plasma. As the pure (2*H*-) MoS_2 for HER electrocatalyst, the as-fabricated 3050 nm additive-free columnar film electrode shows a stable electrochemical activity for HER (an overpotential of 204 mV at a current density of -10 mA/cm^2). Interestingly, the MoS_2 film with controllable thickness can serve as an innovative platform to study the electrocatalytic activity of the customized different active sites (the exposed active edge of sheets (***eE***), stepped-termination surfaces (***sS***) and terrace on the basal planes (***tB***)) and the dependence of electrocatalytic efficiency of the vertically-aligned MoS_2 ***eE*** active sites on their distance to the current collector. The results firstly revealed that the ***tB*** active sites possessed almost the same electrocatalytic activity as that of the ***eE*** active sites but higher than ***sS*** active sites. The electrocatalytic efficiency of the ***eE*** active sites decreased as their distances to the current collector were gradually increasing, due to the limited conductivity of the semi-conductive 2*H*-MoS_2 sheets. This work proposes and evaluates a facile

strategy for replying the question on how to investigate the electrocatalytic activities of various active sites in the electrocatalysts.

KEYWORDS: MoS_2, physically-sputtering strategy, various active sites, electrocatalytic activity, hydrogen evolution reaction

1. INTRODUCTION

In view of the forthcoming fossil fuel exhaustion, rapid global population growth and environmental issues, the immediate deployment and development of renewable energy resources become paramount. Hydrogen fuel is considered to be one of the most promising sustainable and clean energy sources since the raw material for the hydrogen production is water.[1-4] Solar energy is a rival source but with some issues due to the intermittent nature. By comparison, hydrogen fuel can be produced by simply splitting water driven by electrocatalyst and the production process is paralleled. The low abundance and high cost feature of Pt has limited its wide adoption for the hydrogen evolution reaction (HER) even though Pt based electrocatalyst are demonstrated to have the most effective catalysis performance.[4-7] Currently, one challenge is to develop a low cost but high efficiency electrocatalyst, as an alternative to the earth-rare Pt for HER.

The race was started to improve the HER performance of non-noble-metal candidate materials (carbide: W_2C, Mo_2C, etc.;[8,9] phosphide: MoP, Ni_xCo_yP, etc.;[10,11] nitride: Ni_3N, WN, etc.;[12,13] oxide: Co_3O_4,[14] transition metal dichalcogenides (TMDs)[6,7,15,16]) since the natures of their active sites for electrocatalytic activity had been identified. One of the main strategies was to create more active sites per unit area, and the other was to improve the electric conductivity to further enhance the electrocatalytic activities of the existing active sites. Among the aforementioned candidates, the TMDs have been widely studied due to their promising high activity and high stability in many strong acids. Up to now, extensive efforts have been devoted to developing the TMDs (MoS_2, WS_2, $MoSe_2$, WSe_2,

$MoTe_2$, $NbSe_2$, etc.)[7,15,17,18-26] and tailoring their nanostructure (the ratio of effective atoms at the surface and subsurface) to maximize the amount of active sites to ultimately enhance HER performance. The efficient strategy to increase the density of active sites included (i) reduction of the TMDs' size to enlarge the ratio of the exposed active edge of sheets (***eE***),[21,27-29]and (ii) induction of the heterogeneous growth of TMDs crystals to fabricate the stepped-termination surface (***sS***),[7,15,30] and (iii) activating the inert basal plane by creating the active terraces (***tB***),[21,24,31-35] and (iv) switching the semi-conductive 2*H* phase to the metallic and active 1*T'* phase TMDs. [7,36-39] Grain boundary was also known as another type of active site but it had lower electrocatalytic activity than ***eE***, ***sS*** and ***tB***.[40] Thus, additive manufacturing of more active sites in MoS_2 electrode held broad interests and significances to fully accelerate the HER kinetics. Hu et al have simply pointed out that the more loading mass of porous active material in electrode film, the higher hydrogen yield.[17,18] Nevertheless, it was still unclear of the contribution of the high-loading mass active material on the enhanced hydrogen production. The key challenge was in lack of the understanding of the contributions of different active sites on the HER kinetics. David et al have used porous MoS_2 electrodes with various thicknesses as model to identify the dominant factors of active sites for HER activity.[38,41-43] However, it was real no way to define the contribution of the electrocatalysis active sites in the randomly restacked MoS_2 electrode on HER performance by weight, because their relative proportion was unknown and their electrocatalytic activities were also unclear. In fact, the explicit definition of the electrocatalytic activities of various active sites for HER is essential to design the well-defined structure for further enhancing their electrocatalytic performance.

Recently, the novel physical approach is triggering interests in manufacturing the additive-free vertically-aligned active materials on current collector to explore the enhanced electrochemical performances.[44-47] This stimulates us to explore a straightforward physically-sputtering strategy to directly synthesize the porous and ordered TMDs film on the current collector to define electrocatalytic

activities of active sites for HER. There will be no any interference of re-stacking or aggregating by the binder or conductive agents. Considering the MoS_2 as the representative of TMDs, we propose a physical vapour deposition (PVD) strategy to synthesize the ordered MoS_2 films with various thickness (~15 nm to 3050 nm) *via* precisely controlling the sputtering plasma conditions: the ultra-thin *2H*-MoS_2 film with terrace on the basal plane (***tB***), the thin MoS_2 film with exposed stepped-termination surface (***sS***), the vertically-aligned MoS_2 film with abundant exposed active edge (***eE***). The current collector is cleaned carbon fibre (CF). Moreover, in this study, we aim to develop a new approach to reveal the electrocatalytic activities of various active sites in the MoS_2 electrocatalyst for HER performance.

2. EXPERIMENTAL DETAILS

2.1 MoS_2 film electrode deposition

The MoS_2 films were directly fabricated on the CF substrate without any additives by using a magnetron sputtering strategy in the Ar plasma. The source material was 99.99% MoS_2 target with diameter of 75 mm. The maximum fabrication area of film depends on the target size. Before the deposition, the CF substrate was cleaned by acetone for 10 minutes, alcohol for 10 minutes and deionized water (DI) for 5 minutes. The deposition conditions were under Ar pressure of 0.65 Pa, sputtering power of 275 W and CF substrate bias voltage of -30 V. The deposition time of the MoS_2 films with thickness of ~15 nm, ~35 nm, 76 nm, 880 nm and 3050 nm was 40 seconds, 1 minute 30 seconds, 3 minutes, 28 minutes and 100 minutes, respectively.

2.2 Structure characterization

The phase structure of the MoS_2 films was characterized by grazing incidence X-ray diffraction (GIXRD, Philips X'Pert) using Cu K_α radiation under an incident beam angle of 1°, and Raman microscopy (Thermo Scientific, DRX) with an excitation wavelength of 532 nm. The surface and cross-sectional morphologies of MoS_2 films were analysed by field emission scanning electron

microscopy (FESEM, Hitachi SU8230). The cross-sectional structure of representative 3050 MoS_2 film was observed by a high-resolution transmission electron microscope (HRTEM, FEI Titan Themis Cubed 300) and the chemical component was analysed by the attached energy dispersive X-ray spectroscopy (EDS). The Pt/Ir layers were deposited on the as-deposited 3050 nm MoS_2 film to protect the original film structure from any damage by the high energetic focused ion beam (FIB) in the preparation process of cross-sectional TEM sample. The X-ray photoelectron (XPS) spectrum was collected using an XPS (Thermo UK) equipped with mono-chromated Al K_α radiation to further analyse the detailed chemical composition of film.

2.3 Electrochemical measurements

All electrochemical measurements were performed with a standard three-electrode electrochemical cell in 0.5 M H_2SO_4 solution. The Ag/AgCl (3 mol/L KCl), Pt/C rod and as-deposited pure MoS_2 films coated CF electrode were used as the reference, counter and working electrode, respectively. The Ag/AgCl reference electrode was properly calibrated. All potentials reported in this paper were converted to the reversible hydrogen electrode (RHE) by adding a value of (205+59×pH) mV. Polarization curves were acquired by sweeping the potential from 0 to -500 mV *vs.* RHE at a sweep rate of 2 mV/s. Tafel slopes were determined by replotting the polarization curves. Electrochemical impedance spectroscopy (EIS) was performed with frequency from 100,000 Hz to 0.01 Hz and an amplitude of 10 mV under the overpotential of 200 mV *vs.* RHE, and spectra were appraised through the Levenberg-Marquardt minimization procedure. iR_s compensation (current times internal resistance) was applied in all sweep running experiments to account for the voltage drop between the reference and working electrodes, where R_s is the solution resistance extracted from the fitted EIS data. Cyclic Voltammetry (CV) for double layer capacitance measurements was taken in a potential window between 0.1 to 0.2 V (*vs.* RHE) at scan rates of 10, 30, 50, 70, 90, 110 mV/s. The total current density

obtained from the current density difference ($\Delta j = j_a - j_c$) at 0.15 V (*vs.* RHE) was plotted against the scan rate, where the double layer capacitance (C_{dl}) is equivalent to the slope of the fitted line. The electrochemical surface area (ECSA) of a catalyst can be calculated according equation: ECAS= C_{dl}/C_s, where C_s is the capacitance of the sample with an atomically-smooth planar surface material. The overpotential-time responses were detected for 10 hours by chronoamperometric measurements under the current density of -10 mA/cm^2.

3. RESULTS AND DISCUSSION

3.1 Characterization of MoS_2 film electrode

To verify the feasibility of fabricating the porous and ordered MoS_2 film *via* physically-sputtering approach, the structure characterization of the as-prepared film was investigated by the FESEM and focused ion beam (FIB)-HRTEM. **Figure 1**(a) shows the FESEM image of the 3050 nm MoS_2 film on CF. The MoS_2 film covers the top surface of the CF substrate. The FESEM image of as-prepared FIB-TEM sample is shown in **Figure S1**. The cross-sectional TEM images and EDS mapping of the representative 3050 nm MoS_2 film are presented in **Figure 1**(b)-(f). From **Figure 1**(b), it can be seen that the ordered and vertically-aligned columnar MoS_2 platelet film is monolithic, and the porous feature is obvious as well. The seamless connection between film and the CF substrate suggests a good adhesion. The morphologies of MoS_2 films with thicknesses of ~15 nm, ~35 nm, 76 nm, 880 nm and 3050 nm were characterized by FESEM, and the cross-sectional and surface morphologies are shown in **Figure 2**(a). The ~15 nm and ~35 nm MoS_2 films exhibit typical cluster characterization and other films show columnar structure. The later films present the porous surface morphologies. The typical different zones in 3050 nm columnar MoS_2 film (Zone *I*: basal orientation crystal at MoS_2/fibre interface, Zone *II*: the stepped-termination surface and Zone *III:* the continuous columns above the basal crystal) were further characterized and the HRTEM images are presented in **Figures 1**(c)-(e). It

could be seen that the dense MoS_2 layers with ~20 nm thickness are robustly bonded to the substrate surface. The layer-to-layer spacing of 0.65 nm in the S-Mo-S layers clarifies the basal plane of MoS_2 crystals (as shown in **Figure 1**(c)). The terrace stages can decorate the exposed basal crystal plane (Zone *I*) if the film thickness was below ~20 nm, such as the ~15 nm ultrathin MoS_2 film in this study. As the basal crystals grew up (thicker than ~20 nm), they would be was blocked by the growing grain crystals.[48] Thus, the growth direction of edge orientation crystals can switch from being parallel to current collector to being perpendicular to it at the intersection boundaries of crystals. Ultimately the continuous columnar MoS_2 platelets with edge orientation crystal structure can be formed, as shown in **Figure 1**(d). The length of columnar MoS_2 platelets can be easily controlled *via* simply adjusting the sputtering time (see the **Figure 2**(a)). **Figure S2** shows the corresponding selected area electron diffraction (SAED) patterns with strong rings of (100), (103) and (110) MoS_2 crystal planes in the representative columnar MoS_2 platelet zones. It verifies that the edge orientation structure of the entire columnar platelet (Zone *III*) is homogenous in MoS_2 film. The edge of the MoS_2 columnar platelets are always decorated by abundant active edge sites, as previously reported.[21,27,28,48]

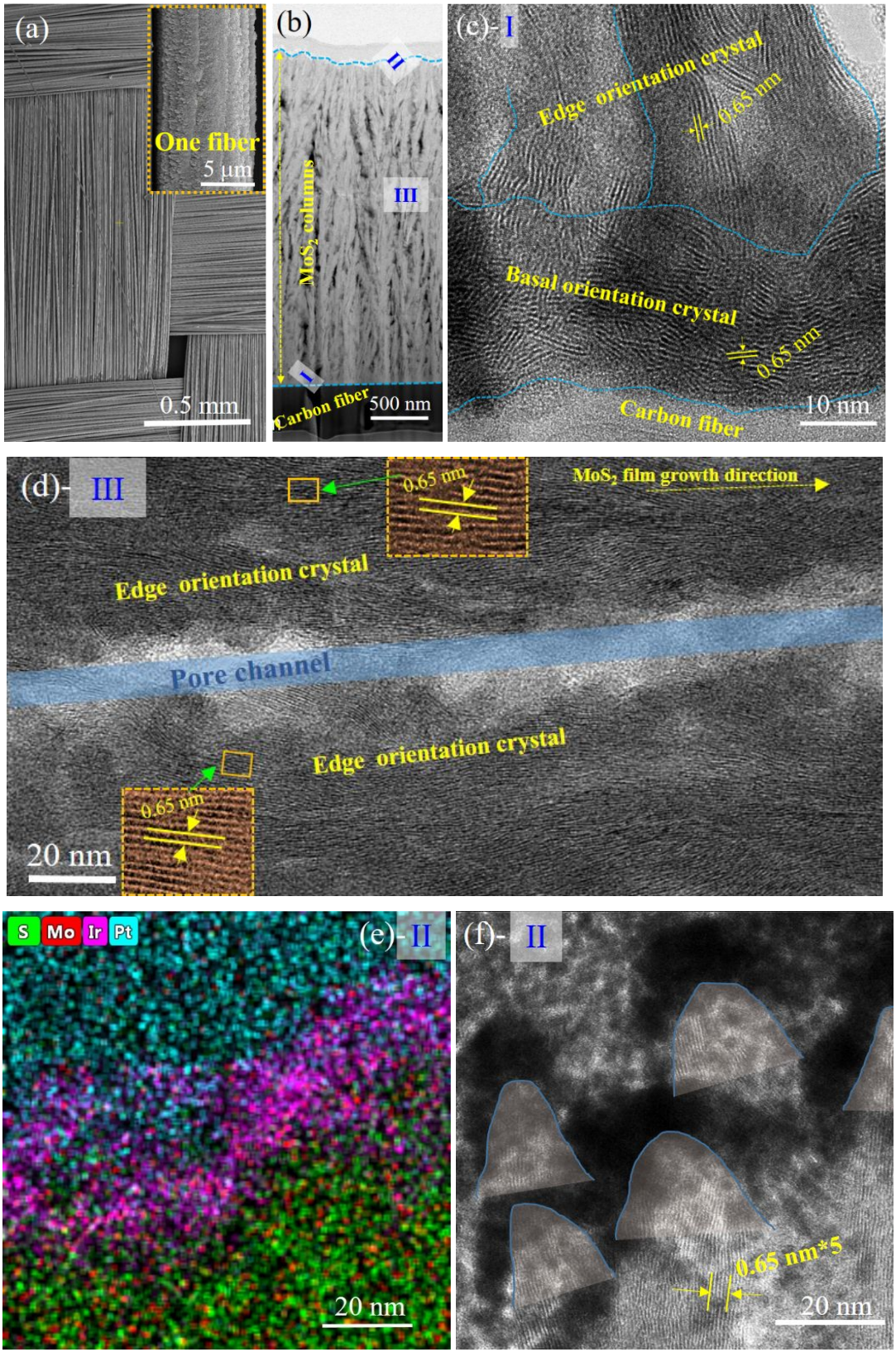

Figure 1. (a) The FESEM image of 3050 nm MoS_2 film on CF substrate (the inset is one fibre), (b) cross-sectional HAADF image of 3050 nm MoS_2 film on CF, cross-sectional HRTEM images of Zones

I (c) and III (d) in panel (b), and the combined EDS elemental mapping (e) and cross-sectional HRTEM image (f) of Zone II in panel (b).

The Pt/Ir layers were initially utilized to protect the original film surface structure of FIB sample. As shown in **Figure 1**(e), the wavy distribution of coated Ir element on the top of 3050 nm MoS_2 film suggested the top surface (Zone *II*) was very rough. The marked stepped-termination surfaces of each columnar MoS_2 platelet are shown in **Figure 1**(f) and **Figure S3**(a),(b). They are another type of active sites for the outstanding HER performance, as previously reported.[7,15] The height of the formed stepped-termination surfaces of each columnar MoS_2 platelet was 15~20 nm, as shown in **Figure 1**(f).

The chemical composition and structure of the *2H*-MoS_2 phase were further investigated by XPS and Raman microscope, respectively, and the results of representative 3050 nm MoS_2 film are presented in **Figure 2**(b)-(d). The XPS spectra were calibrated by a carbon 1*s* peak located at 284.8 eV. The Mo^{4+} $3d_{5/2}$ and $3d_{3/2}$ peaks, the S^{2-} $2p_{3/2}$ and $2p_{1/2}$ peaks in XPS spectra were located at 229.0, 232.2, 161.8 and 163.0 eV, respectively, (**Figure 2** (b),(c)) representing the *2H* structure of the as-fabricated MoS_2 in this study.[38,49,50] As shown in the Raman spectrum in **Figure 2**(d), it is consisted of two main Raman modes of E^1_{2g} and A_{1g}, and the distinct J_1, J_2 and J_3 peaks for 1T'-MoS_2 phase are absent, indicating that pure *2H*-MoS_2 phase was ultimately formed by the physically-sputtering strategy in this study.

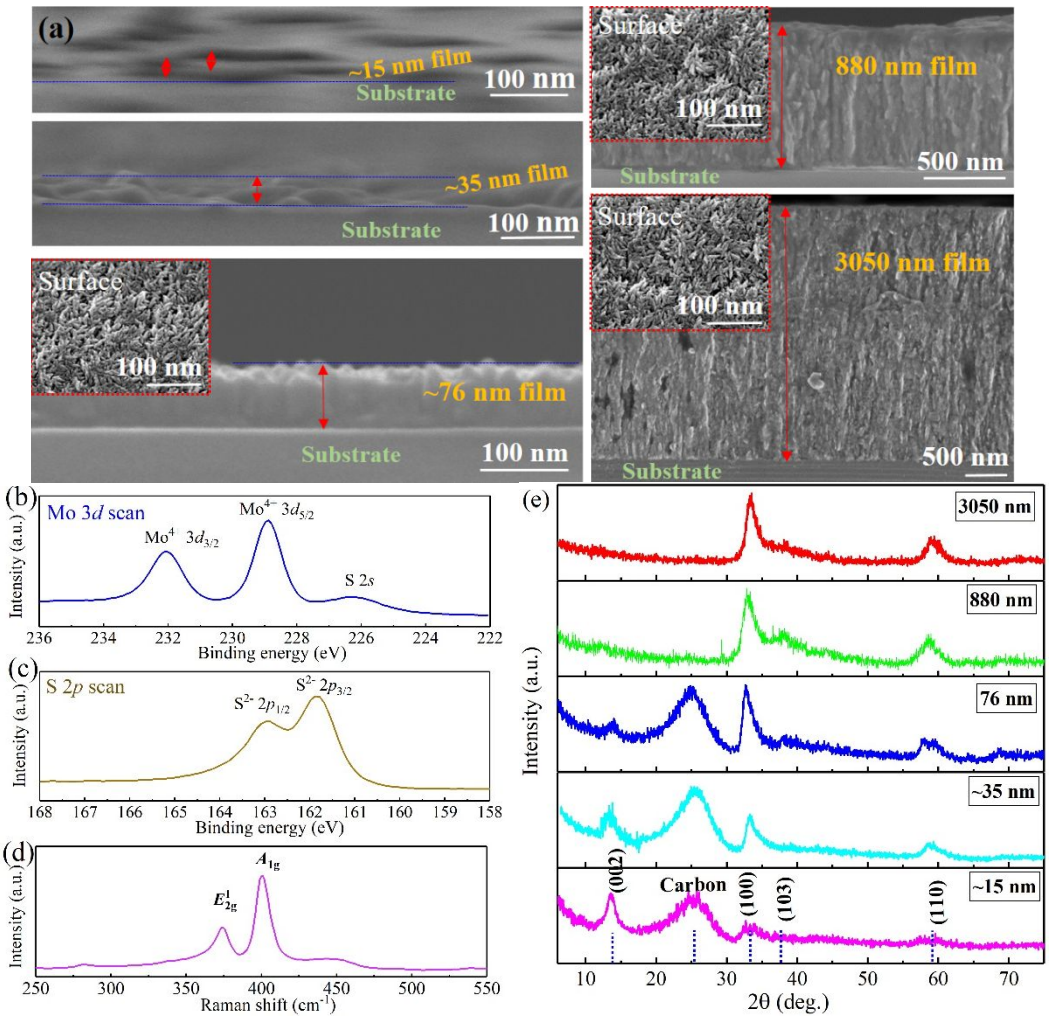

Figure 2. (a) The FESEM images of the cross-sectional and surface morphology of MoS_2 films with thickness of ~15 nm, ~35 nm, 76 nm, 880 nm and 3050 nm, respectively. The high resolution XPS scans of (b) Mo 3*d* and (c) S 2*p* and (d) Raman spectrum of the 3050 nm MoS_2 film. (e) GIXRD spectra of MoS_2 films on CF.

Here, we aim to evaluate the electrocatalytic activity of various active sites in MoS_2 electrode. To identify typical crystal characterization of the MoS_2 films which are decorated by different active sites, the GIXRD measurement of films was performed and the pattern spectra are shown in **Figure 2**(e). Apart from the diffraction peak from the carbon fibre (CF) substrate located at 25.8°, the peaks associated with (002), (100), (103) and (110) orientation of the 2*H*-MoS_2 crystal are observed.[7,38] The strongest (002) diffraction peak of the ~15 nm MoS_2 film indicated that the deposited MoS_2 crystal clusters were the dominant basal orientation. In the ~35 nm MoS_2 film, the intensity ratio of $I_{(100)}/ I_{(002)}$

rose. It should be due to the switch of orientated-growth from the dominant (002) plane to (100) plane as the maximum thickness of basal planes reached up to ~20 nm (as shown in **Figure 1**(c)). The morphological feature of 2*H*-MoS_2 (100) plane is columnar. With further growth of the MoS_2 columnar platelets (76 nm thickness), the diffraction signal of the (002) plane was further weakened due to the shielding of the formed thick (100) and (110) crystals with columnar morphology. As the thickness of column-dominated MoS_2 film was up to 880 nm, the (002) crystal plane and CF disappeared accompanied by the significant rising of the MoS_2 (100) and (110) crystal planes with edge orientation. The diffraction patterns of 880 nm and 3050 nm MoS_2 films are almost same, indicating that the structure of the MoS_2 columnar platelets was independent on the platelets' length. All the column-dominated MoS_2 films are decorated by the stepped-termination edges at their top surfaces (shown in **Figure 1**(f)).

Therefore, it can be stated that the exposed different active sites of the MoS_2 film can be additively manufactured by this on-step physically-sputtering approach *via* controlling the film thickness. This physically-sputtering strategy should be scalable to fabricate the large area of films on diverse substrate surface and the maximum loading area depends on the volume of the sputtering chamber. The pure mass of 3050 nm MoS_2 film per area is about 0.96 $mg \cdot cm^{-2}$ and the density is found to be 3.15 $g \cdot cm^{-3}$. The calculated porosity is 37.7 % (taking the MoS_2 density to be 5.06 $g \cdot cm^{-3}$). The columnar pores are expected to provide free access channels for the electrolyte to the internal active sites of the columnar MoS_2 film. Theoretically, the immature basal plane-dominated MoS_2 film (~15 nm) was in abundance of exposed ***tB*** active sites, the infantile columns on the matured basal planes of the MoS_2 film (~35 nm) was in abundance of ***sS*** active sites and the column-dominated MoS_2 films (76 nm, 880 nm and 3050 nm) were rich of two kinds of ***eE*** and ***sS*** active sites**.**

3.2 Fundamental Theory of the MoS_2 film growth in plasma

Numerous density functional theory (DFT) calculation and experimental investigation results have determined that the terraces on the MoS_2 basal plane (***tB***), the exposed active edge sites (***eE***), and the stepped-termination surface (***sS***) of MoS_2 sheets facilitated not only the adsorption of H^+ from intermediate but also the desorption of hydrogen product for the high HER performance. [7,15,31,51-54] The schematic illustration of physically-sputtering strategy and the distribution of the various formed active sites (***eE***, ***sS*** and ***tB***) along MoS_2 film growth direction is shown in **Figure 3**. On basis of the classic Thornton model and aforementioned analysis of as-fabricated MoS_2 films, the growth mechanism of MoS_2 film consists of two main steps: (i) the initial formation of thin basal orientated MoS_2 crystal planes on substrate (CF), and (ii) the following formation of the edge orientated MoS_2 crystal platelets, in which various active sites were speculated to distribute in different height zones of MoS_2 film.[55,56] Precisely-tailoring the MoS_2 target power density is essential to create kinetic Mo and S atoms for their indispensable migration in plasma and adsorption on the growing surface to ultimately fabricate the structure controllable MoS_2 film.[57,58] During the film growth process, in comparison to the low surface energy (~250 $mJ \cdot m^{-2}$) and high activation energy (~120 $kJ \cdot mol^{-1}$) of sulphur (002) basal plane, the high surface energy ((100) plane of ~250,000 $mJ \cdot m^{-2}$) and low activation energy of ((100) plane of 95 $kJ \cdot mol^{-1}$) surface diffusion edge plane could prevent the desorption of incident Mo and S ions and promote the growth of edge plane.[59,60-62] In other words, the interfacial energy between the MoS_2 basal plane and substrate is much higher than that between the edge plane and substrate.

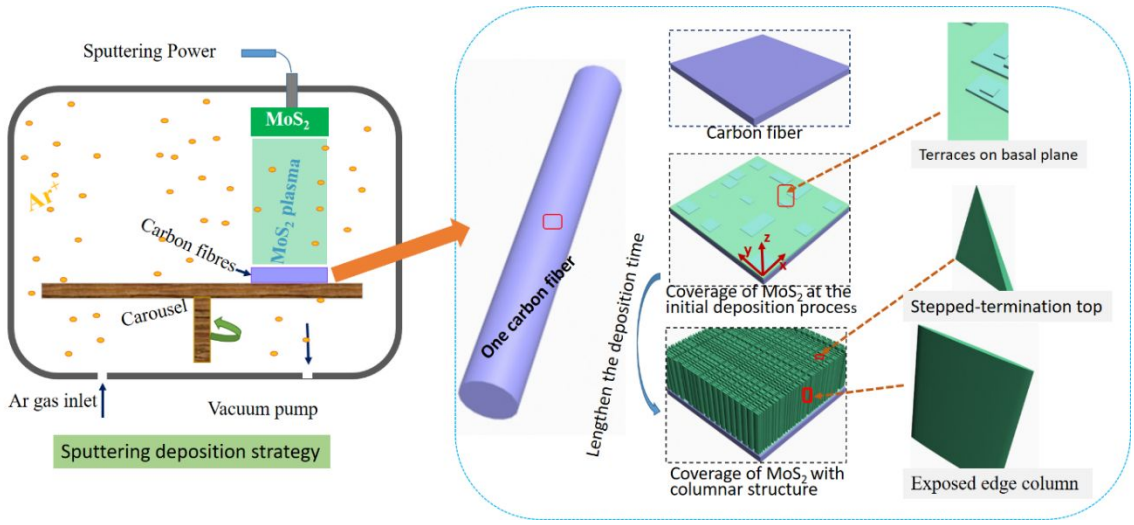

Figure 3. The fabrication strategy of MoS_2 films with various active sites on the carbon fibre.

In the initial growth stage, the abundant absorbed MoS_2 atoms on rough surface could promote 2D nucleation and the rapid growth of MoS_2 edge planes parallel to substrate surface. Meanwhile, the growth of MoS_2 edge planes perpendicular to substrate surface was limited. Thus, the MoS_2 basal orientated growth and rapid extension of edge plane parallel to the substrate surface were synchronous, and ultimately the polycrystalline MoS_2 with basal orientation was formed in the thin MoS_2 film (~15 nm MoS_2 in this study). The abundant terrace (***tB***) was formed on the immature basal planes before they grow up (~15 nm MoS_2 in this study). The basal plane nuclei would bond with each other at their domain boundaries when they grew up.[21,48,54,55,63]

In the second growth stage, the mutually-blocking effect of adjacent edge orientated crystals can facilitate the crystal to grow vertically at the boundaries because of the more free geometry space in the vertical direction upward. Furthermore, the high surface energy (2 orders of magnitude larger than the basal plane) and low surface activation energy of edge plane determined the edge orientation growth, resulting in formation of the columnar platelet structure, which were always decorated by abundant active edge sites (***eE***).[48,57,60,63] It can be also stated that the different growth rate of each S-Mo-S layer resulted in the uneven edge orientated columnar platelets.[7,15,30] In other words, the stepped-termination

surfaces (***sS***) were ultimately formed. The concomitantly-formed vertical pores around the columnar MoS_2 platelets can enable the free access of electrolyte to the internal of the electrode, allowing active sites to fully expose to electrolyte.[41,48] The energetic plasma atmosphere, as optimized in this study, is essential for the staged-growth of MoS_2 films: the initial growth of MoS_2 basal plane with abundant ***tB*** (below ~20 nm thickness) and subsequent growth of MoS_2 edge plane with abundant ***eE*** and ***sS***.

3.3 Insights into electrocatalytic activities of various active sites of 2*H*-MoS_2 for HER

The typical polarization curves of MoS_2 films decorated by different type of active sites are shown in **Figure 4**(a). The ~15 nm MoS_2 film gives a high overpotential of 386 mV *vs* RHE at a current density of -10 mA/cm^2, which is lower than that of the ~35 nm MoS_2 film with the stepped-termination surface (432 mV *vs* RHE). For the column-dominated MoS_2 films, the thicker the MoS_2 film, the greater HER activity can achieve: as the thickness of the columnar MoS_2 film increased from 76 nm to 880 nm, and further to 3050 nm, the HER activities are boosted with the overpotential as low as 342 mV *vs* RHE, 280 mV *vs* RHE and 204 mV *vs* RHE, respectively. The improved electrocatalytic activity of 3050 nm (2*H*-) MoS_2 should be attributed to the porous and vertically-aligned MoS_2 film with large specific surface area and abundant exposed active edge sites.[17,41] It is worthy to further elucidate both the electrocatalytic activity and efficiency of the difference active sites in the MoS_2 electrode for HER.

The Tafel slope is used to evaluate the dominant HER mechanism of the cathodic electrode/electrolyte interface in the low current range. As shown in **Figure 4**(b), the Tafel plots of the ~15 nm, ~35 nm, 76 nm, 880 nm and 3050 nm films and Pt/C are 136 mV/dec, 159 mV/dec, 128 mV/dec, 123 mV/dec and 125 mV/dec, and 37 mV/dec, respectively. As reported by Tributsch and Carway et al.[41,64,65], the Tafel slope of ~120 mV/dec was generally observed as the surface coverage of the adsorbed hydrogen, H_{ads} (H*), on the electrode was relatively low. Thus, the Volmer reaction mechanism

$$H_3O^+ + e^- + * \rightleftarrows H^* + H_2O$$

is the rate-dominating step (*RDS*) of MoS_2 film for HER in this work. In this equation, the * indicates the catalytic active sites. It is still unclear which is the dominant factor for the limited formation of H* on the active sites: is it the small amount of active sites, the limited electron transfer ability through the active materials or the low supply capacity of H_3O^+ to the internal active site from electrolyte? Until now, there are still no consensus on this dominant factor on the unremarkable hydrogen reaction kinetics, associated with Tafel slope in the range of 100~145 mV/dec for 2*H*-MoS_2.

To elucidate the electrocatalytic activity of active site, the basal orientated plane at the interface was defined as Zone *I*, the stepped-termination surface was defined as Zone *II,* and the columnar platelet edge was defined as Zone *III* (shown in **Figure 1**(b) and **Figure 4**(c)). The ~15 nm film possesses the immature basal planes decorated by terrace active sites (***tB***), and the ~35 nm film constitutes of Zone *I* with thickness of ~20 nm and the upper Zone *II* (~15 nm) with ***sS*** active sites*,* in which the Zone *I* was covered by the upper Zone *II*. The film with thickness over 76 nm constitutes of the bottom Zone *I* with thickness of ~20 nm (as illustrated in **Figure 1**), the topmost ~15 nm thickness Zone *II* with ***sS*** active sites and the middle columnar Zone *III* with ***eE*** active sites, in which the Zone *I* surface was covered by the Zone *III*. Based on the aforementioned analysis, the electrocatalytic activities of MoS_2 were attributed to the terrace sites on the immature basal planes (***tB***) for ~15 nm MoS_2 film, uncovered stepped-termination surface sites (***sS***) for ~35 nm MoS_2 film, and both the exposed edge sites of the columnar platelets (***eE***) and uncovered stepped-termination surface sites (***sS***) for 76 nm MoS_2 film, respectively. The operating overpotential of 400 mV *vs RHE* was selected as one representative evaluation criterion in this study. From the **Figure 4**(b), it can be found that the ~15 nm MoS_2 film's Tafel slope (136 mV/dec) is lower than that of ~35 nm MoS_2 film (169 mV/dec), and the current density (12 mA/cm^2 at 400 mV vs RHE) is higher than that of ~35 nm MoS_2 film (8 mA/cm^2 at 400 mV vs RHE). It indicates that the electrocatalytic activity of terrace sites on the immature basal plane (***tB***) is higher than the stepped-termination surface sites (***sS***).

With further increase in film thickness, the columnar Zone *III* of MoS_2 film grew up. Thus, the Zone *III* of the 880 nm MoS_2 film can be further divided into Zone III_{41} and Zone III_{804}, and Zone *III* of the 3050 nm MoS_2 film can be further divided into Zone III_{41}, Zone III_{804} and Zone III_{2176}. The Tafel slope of 76 nm MoS_2 film should be considered as a mixture of the columnar Zone III_{41} and short stepped-termination surface Zone *II*, while the proportion of Zone *II* was approximate 0 in the mixed Tafel slope value as the columns were up to the length of 880 nm and 3050 nm MoS_2 films. The similarity of Tafel slopes of the ~15 nm film and the column-dominated films (880 nm and 3050 nm MoS_2 films) verified that the terrace active sites on the immature basal planes and active edge sites on columnar platelet edge possess the same electrocatalytic activity for HER. This is the first evidence for elucidating the HER activity of 2*H*-MoS_2 with diverse active sites *via* tailoring the mono-/di-/tri-types of active site in each film.

It is well worth to further evaluate the electrocatalytic efficiency of ***eE*** active sites in MoS_2 films. Taking the current density at the given overpotential of 400 mV *vs* RHE as an example (J(400 mV)), the J_I(400 mV) value of ~15 nm MoS_2 film represents the electrocatalytic efficiency of Zone *I* terrace sites on basal plane (***tB***). The J_{II}(400 mV) value of ~35 nm MoS_2 film represents the electrocatalytic efficiency of ~15 nm thickness Zone *II*'s stepped-termination surface (***sS***) because the matured ~20 nm thickness basal plane layer was covered by upper Zone *II* during film deposition process in plasma, as shown in **Figure 1**(c). The difference of the two values of 76 nm film and the ~35 nm film, ∇J_{III41}(400 mV), represents the electrocatalytic efficiency of Zone *III* edge sites along columnar platelets with 41 nm length (Zone III_{41}), and the difference of the two values of the 880 nm film and the 76 nm film, ∇J_{III804} (400 mV), represents the electrocatalytic efficiency of Zone *III* edge sites along the columnar platelets with further 804 nm length (Zone III_{804}), and the difference of the two values of the 3050 nm film and the 880 nm film, $\nabla J_{III2176}$ (400 mV), represents the electrocatalytic efficiency of Zone *III* edge sites along the columnar platelets with further 2176 nm length (Zone III_{2176}). **Figure** 4(d) presents the

current density of the defined zone of the MoS_2 film at the given overpotential of 400 mV vs *RHE*. It is obviously observed that the Zone *I*, Zone *II* and Zone III_{41} exhibit the low current density of 11.9 mA/cm^2, 8.1 mA/cm^2 and 11.0 mA/cm^2, respectively. They are much lower than those of the far column zones of ∇J_{III804} (400 mV) and $\nabla J_{III2176}$ (400 mV), which are 20.2 mA/cm^2 and 42.8 mA/cm^2, respectively. It suggested that large amount of ***eE*** active sites of MoS_2 are contributed to the high electrocatalytic efficiency for HER.

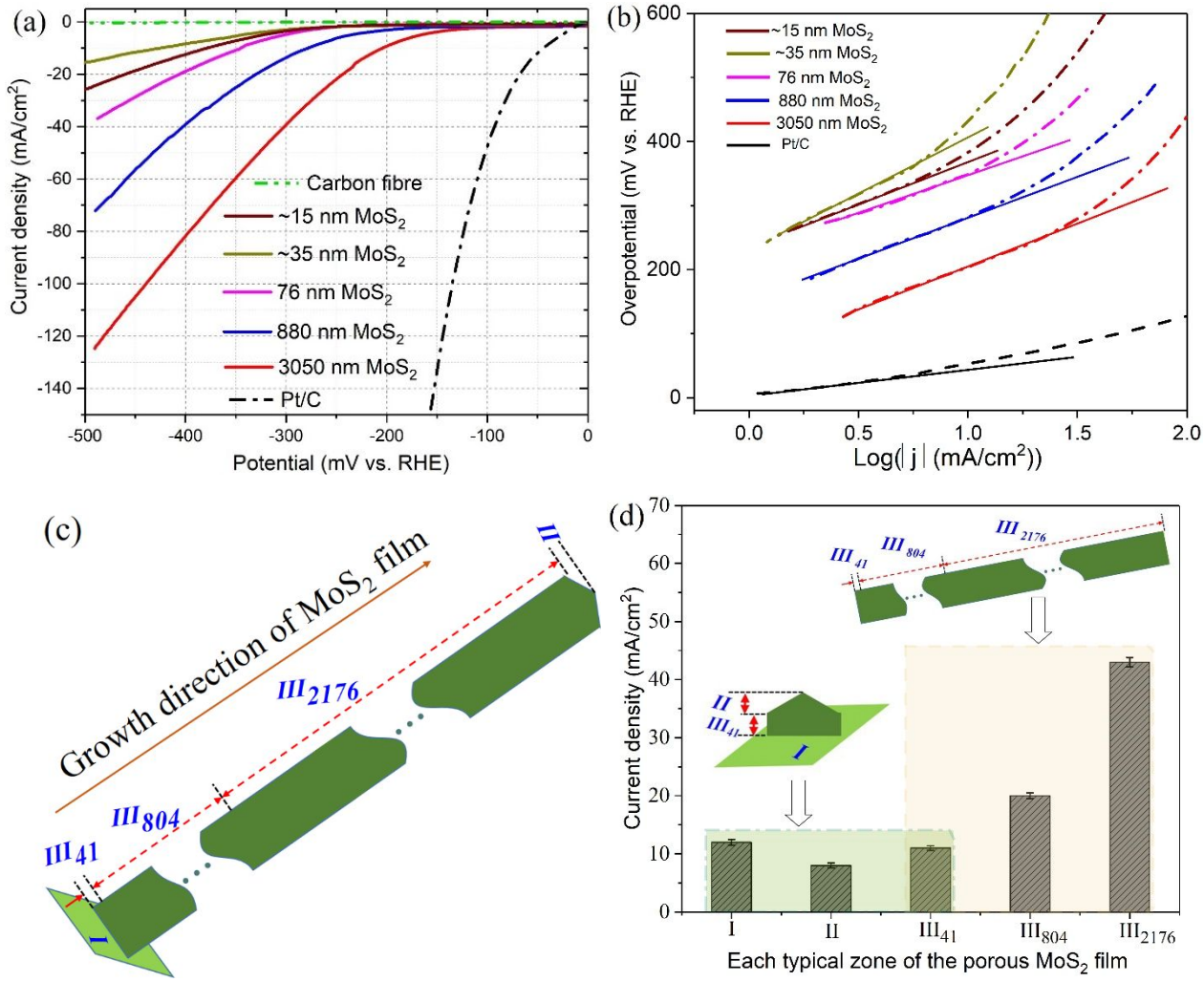

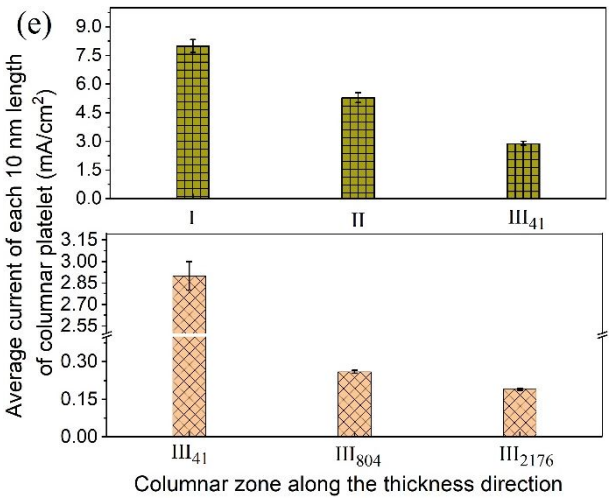

Figure 4. Electrochemical measurements for the MoS_2 film on CF in 0.5 M H_2SO_4: (a) Polarization curves for MoS_2 films with different thickness at a scan rate of 2 mV/s, (b) Tafel plots for the MoS_2 films, (c) the illustration of the typical active zones along the height of the 3050 nm MoS_2 film, (d) the current density of different active zones under the overpotential of 400 mV *vs RHE* and (e) the corresponding current density of each 10 nm length of the active zones.

Since the Zone *I* of ~15 nm film, Zone *II* in ~35 nm film and Zone *III*$_{41}$ in 76 nm film have the same order of magnitude of distance to the current collector, the difference of charge transport in these three zones can be negligible and the active site activity should be considered to be the dominant factor for the electrocatalytic efficiency. Taking the current density of each 10 nm length of the active Zones *I*, *II* and *III* as the standard of comparison, the electrocatalytic efficiencies of the typical active zones were further investigated at the given overpotential of 400 mV *vs* RHE, as shown in upper of **Figure 4**(e). The results show that the current density of each 10 nm length Zone *I* (in abundance of terrace active sites (***tB***)) is 7.9 mA/cm^2·10 nm^{-1}, substantially higher than those of the Zone *II* of stepped-termination surface active site (***sS***) and Zone *III* of exposed edge site (***eE***), which are 5.3 mA/cm^2·10 nm^{-1} and 2.9 mA/cm^2·10 nm^{-1}, respectively. Lots of previous reports have already demonstrated the electrocatalytic activity of terraces on basal plane (***tB***), the stepped-termination surface (***sS***) and column edge site (***eE***) of vertically-aligned MoS_2, but it is the first time to properly compare their electrocatalytic activity and efficiency. Increasing the length of columnar platelets would increase the amount of available

electrocatalytic sites at the edge of columnar platelets (***eE***), enabling the high current density at a given overpotential of 400 mV *vs* RHE, as shown in **Figure 4**(d). Nevertheless, the current density of each 10 nm length of the Zones III_{41}, III_{804} *and* III_{2176} decreases gradually from 2.90 mA/cm^2·10 nm, to 0.26 mA/cm^2·10 nm and then 0.19 mA/cm^2·10 nm at the given overpotential of 400 mV vs RHE, as shown in the bottom of **Figure 4**(e). The similar current density evolution trends of the different active site zones (Zones III_{41}, III_{804} *and* III_{2176}) are also observed under the given overpotential of 350 mV vs *RHE* (**Figure S4**) and 450 mV vs *RHE* (**Figure S5**), respectively. It is immediately apparent that the current density of MoS_2 columnar platelets is distance dependent: edge active sites far away from the current collector have a low yield of hydrogen product as the distance gradually increases from dozens of nanometers, to hundreds of nanometers and further to thousands of nanometers scale. By aid of the controllable gradient thickness of MoS_2 film electrodes, it can be further demonstrated that the increase in distance of ***eE*** active sites to the current collector by one or two orders of magnitude (from dozens of nanometers to hundreds of nanometers, and further to thousands of nanometers) reduces the HER electrocatalytic current by about one order of magnitude (**Figure S6**). It can be considered to be further exploration of quantitative correlation of the electrocatalytic activity with dependence of distance to the current collector.[32]

Practically, the electrocatalytic activity was sensitively associated with (i) the exposed active site density, (ii) the energetic adsorption of key reaction intermediates (H^+) and desorption of the reaction product on the active sites and (iii) the charge and proton transfer from the current collector to each active site.[3,7,15,65] The electrochemical double layer capacitance (C_{dl}) is expected to be linear proportional to the electrochemical surface area (ECSA) of porous MoS_2 film, which method was employed to study the distribution of the active sites for HER.[7,38,66] It have been previously proved that the columnar structure was independent on the MoS_2 platelets' length. So the amount of the exposed active sites is linearly proportional to the surface area of columnar platelets even though the surface

active sites are only one part of the entire surface involved. Thus, the comparison of the relative density of the exposed active sites of Zones III_{41}, III_{804} *and* III_{2176} can be still estimated *via* the ∇C_{dl}. The original C_{dl} values were estimated through linear fitting the plot of the current density difference ($\nabla j = j_a - j_c$) at overpotential of 150 mV *vs* RHE *versus* the scan rate. The ∇C_{dl} values of the MoS_2 columnar platelets at Zone III_{41}, Zone III_{804} and Zone III_{2176} can be further estimated through the ∇j_{III41}, ∇j_{III804} *and* $\nabla j_{III2176}$ values *versus* the scan rate, in which the ∇j_{III41} value is the different ∇j values between the 76 nm and ~35 nm films, ∇j_{III804} value is the different ∇j values between the 880 nm and 76 nm films and $\nabla j_{III2176}$ value is the different ∇j values between the 3050 nm and 880 nm films, respectively (The raw data are presented in **Figure S7**). On basis of these, the calculated ∇C_{dl_III41}, ∇C_{dl_III804} *and* $\nabla C_{dl\_III2176}$ values can be utilized to compare the exposed electrochemical surface area of the columnar MoS_2 platelets, as shown in **Figure 5**(a). The ∇C_{dl} value increases from 0.31mF/cm^2, to 7.66 mF/cm^2 and further to 19.3 mF/cm^2 with gradual increasing in the length of columnar MoS_2 platelets from 41 nm, to 804 nm and 2176 nm. As the ∇C_{dl} value of each 10 nm length of MoS_2 columnar platelets was further compared, it can be seen that all the $\nabla C_{dl\_III41\_10}$ (7.56×10^{-3} mF/cm^2), $\nabla C_{dl\_III804\_10}$ (9.48×10^{-3} mF/cm^2) and $\nabla C_{dl\_III2176\_10}$ (8.87×10^{-3} mF/cm^2) values are in the same order of magnitude (as shown in **Figure 5**(b)). It indicates that all the columnar zones *III* have the similar electrochemical surface area, namely, the homogeneously-distributed active sites on the columns' edge, which should not be the dominant factor responsible to the gradually-reduced current density of each 10 nm length columnar MoS_2 platelet as they were gradually far away from the current collector. The current density of each 10 nm length of MoS_2 columnar platelets under a given overpotential of 400 mV *vs* RHE, normalized with the ECSA,[7] are 15.30 mA/cm$^2\cdot$10 nm (Zone III_{41}), 1.07 mA/cm$^2\cdot$10 nm (Zone III_{804})and 0.86 mA/cm$^2\cdot$10 nm (Zone III_{2176}). This ECSA-normalized current densities indicated

the real electrocatalytic efficiency of the MoS_2 columnar platelets is distance dependent: the farther from the current collector the active site is, the lower catalytic efficiency it has.

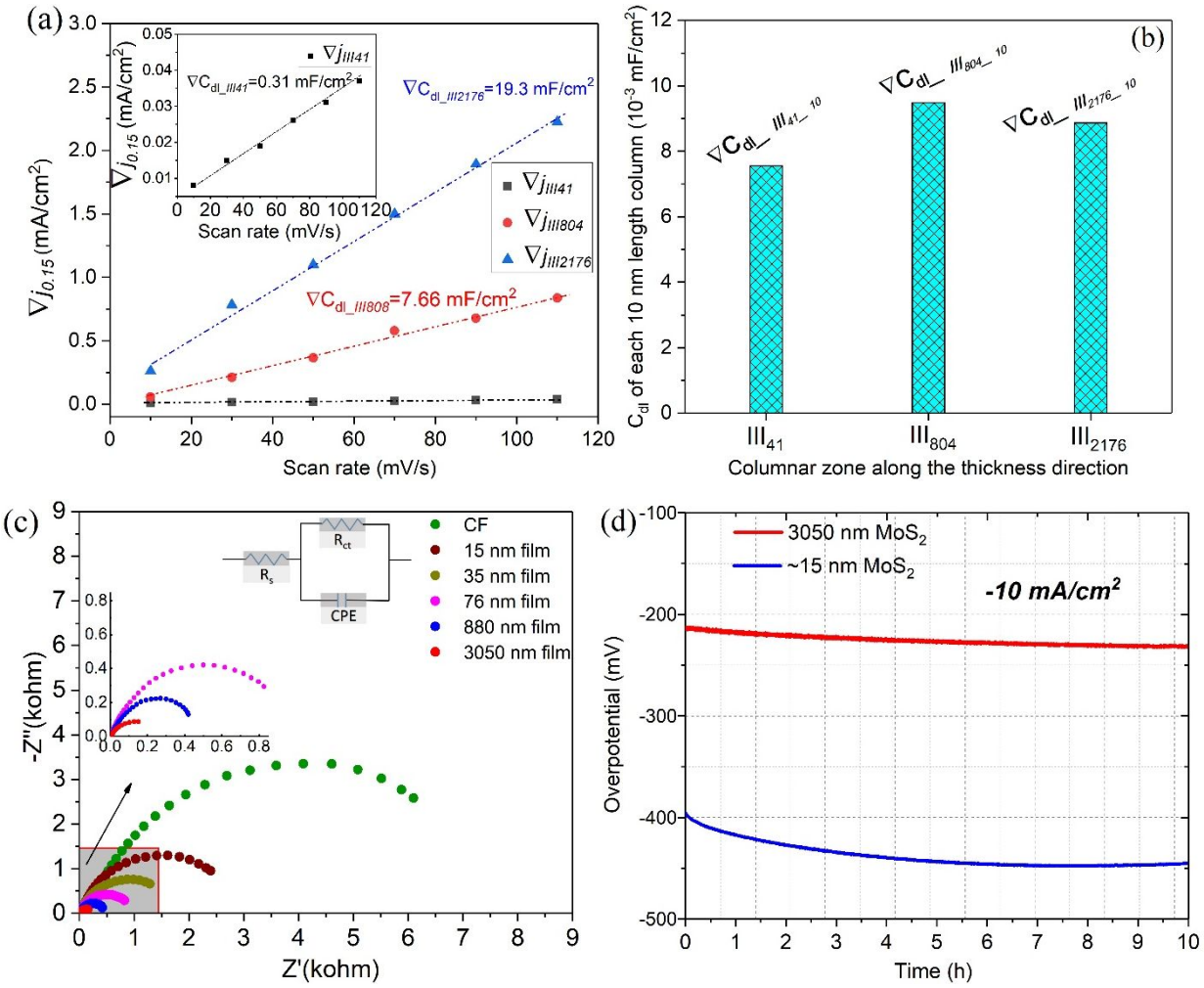

Figure 5. Electrochemical characterization of MoS_2 films on CF: (a) charge-current density difference plotted against the scan rate of the MoS_2 films (C_{dl} is equivalent to the slope of the fitted line), (b) the ∇C_{dl} of each 10 nm length of different *zone III* along the length of the MoS_2 columns, (c) Nyquist plots showing EIS spectra measured at the overpotential of 200 mV *vs* RHE with real (Z′) and imaginary (Z′′) components and (d) chronopotentiometry responses (η~t) recorded from 3050 nm and ~15 nm films at current density of -10 mA/cm^2.

The electrochemical impedance spectroscopy (EIS) was further performed to confirm the rate-dominating step (*RDS*) for the gradual reduction of current density along the length of the columnar platelets, the spectra are shown in **Figure 5**(c) and the R_{ct} values are listed in **Table S1**. The semicircles

are observed in the low frequency regime from the Nyquist curves, which can provide us the dominating step information on the surface exchange process of intermediate and the hydrogen product in HER. The absence of Warburg impedance suggested that mass transport for supplying the H_3O^+ to the active sites was fast, which conclusively suggested that charge transfer was the *RDS* in HER.[15,41] Furthermore, the thick MoS_2 film has a small semicircle, namely, the low charge transfer resistance. This was attributed to the increased internal platelet edge surface of the elongated porous and columnar MoS_2 film which was fully exposed to the intermediate. In this case, the intermediate can be accessible to the internal active sites along the vertical pore channels of film, ensuring the increased interaction between internal active sites with the reactants. It was demonstrated that the conductivity of the in-plane MoS_2 (columnar crystals) was 1,000 times higher than that of out-of-plane.[41,67,68] However, on basis of aforementioned results in this study, it can be stated that the vertical-aligned columnar MoS_2 crystal platelet with abundant active edge sites can't fundamentally change the overall *2H*-MoS_2 semi-conduction characterization or the limited charge transfer capacity either. The low conductivity is still the barrier for the *2H*-MoS_2 to achieve complete interaction of far-end active sites with the as-absorbed H_3O^+, due to the inefficient electron supply. Thus, the zone *III* of columnar platelet far away from the current collector presents low electrocatalytic activities (**Figure 4** (e)). The farther the active site is, the lower electrocatalytic activity it has.

Furthermore, the electrocatalytic stability of the physically-deposited MoS_2 electrodes was measured at the fixed current density of -10 mA/cm^2. The typical chronopotentiometry response curves of the thickest 3050 nm MoS_2 film and the thinnest ~15 nm MoS_2 film are shown in **Figure 5**(d). The results show a more stable and low overpotential for the 3050 nm MoS_2 film electrode. To maintain the cathodic current density of -10 mA/cm^2, the electrode overpotential for 3050 nm MoS_2 film increases from 213 mV to 232 mV (8.2 % fluctuation) over the duration of 10 hours. The 3050 nm MoS_2 film was still pinning on CF substrate after running 10 hours, as confirmed by FESEM image and the EDS

elemental mapping measurement in **Figures S8**(a)-(d). For the ~15 nm MoS_2 film, the overpotential increases from 394 mV to 445 mV (11.4 % fluctuation) to maintain the current density of -10 mA/cm^2. The low fluctuation of electrochemical performance indicated the physically-deposited MoS_2 films could serve as a robust platform to deeply reveal the *RDS* of electrocatalytic mechanism for HER. This new approach proposes and evaluates a new insight on how to investigate the electrocatalytic activities of various active sites in MoS_2 electrocatalyst. Our further research plan is to present how to arrange the conductive agent along the edge-orientated columnar platelets but without any cover or passivate the active sites to fast transfer electron to the far-end active sites, to approach its intrinsic activity rate for HER.

4. CONCLUSIONS

The porous and ordered MoS_2 film with various active sites (exposed edge of columnar sheets (***eE***), stepped-termination surface (***sS***) and terraces on basal plane (***tB***)) was successfully fabricated on carbon fibre by one-step physically-sputtering strategy in energetic plasma environment. The amount of active sites at the edge of columnar platelets can be customized *via* simply controlling the length of the 2*H*-MoS_2 columns. This new approach proposes and evaluates a facile strategy to investigate the electrocatalytic activities of various active sites (***eE***, ***sS*** and ***tB***) and the dependence of ***eE***s' electrocatalytic activities on the distance to the current collector in columnar MoS_2 platelets electrocatalyst for HER. The results reveal that the ***tB*** active site has the same electrocatalytic activity to the ***eE*** active site but it is higher than that of ***sS*** active site. The electrocatalytic efficiency of the ***eE*** active sites at the columnar platelet edge decreased gradually as their distances to the current collector were gradually increasing, from dozens of nanometers to hundreds of nanometers and further to thousands of nanometers scale. It should be attributed to the limited charge transfer from the current collector to the far-end active sites of the MoS_2 columnar crystal platelets. In comparison to the previously-reported pure *2H*-MoS_2 for HER, the physically-deposited *2H*-MoS_2 films can serve as a

robust platform to deeply reveal the *RDS* of electrocatalytic mechanism for HER. As one reference, we believe that this strategy can be employed as a model for the porous and ordered active material to study the electrocatalytic activities of various active sites for HER or/and oxygen evolution reaction.

ASSOCIATED CONTENT

Supporting Information

The Supporting Information is available free of charge on the ACS Publications website at ///

FESEM image of FIB sample; SAED patterns along the thickness direction of cross-sectional 3050 nm MoS_2 film; cross-sectional HAADF image of stepped-termiation surface of columnar platelets; current densities of each 10 nm length column along the thickness direction; cycle voltammogram (CV) curves; FESEM image and EDS mapping of the 3050 nm films after running over 10 hours.

AUTHOR INFORMATION

Corresponding Author

*Yanan Wang: ynwang@licp.cas.cn.

*Anne Neville: a.neville@leeds.ac.uk.

ORCID

Shusheng Xu: 0000-0002-3675-3309.

Jiao Xu: 0000-0002-4812-4622.

Yanan Wang: 0000-0001-8491-8123.

Anne Neville: 0000-0002-6479-1871.

Author Contributions

#Shusheng Xu and Jiao Xu contributed equally to this work. Shusheng Xu, Anne Neville, Yanan Wang conceived the ideas, designed the research and oversaw the entire research. Jiao Xu, Zewen Duan and

Shusheng Xu synthesized the electrocatalysts and conducted the electrochemical measurements, Yu-Zhen Liu, Yanan Wang, Yong Hua and Xiaomin Gao characterized the electrocatalysts.

Notes

The authors declare no conflict of interest.

ACKNOWLEDGEMENTS

The authors are grateful for the financial support provided by Engineering and Physical Sciences Research Council (EPSRC, Grant No. EP/R00496X/1) in the United Kingdom, and National Natural Science Foundation of China (Grant No. 51505465 and 51575508). We also would like to thank the helpful FIB and TEM tests by Mr. John Harrington, Mrs. Zebeada Aslam and Mr. Stuart Micklethwaite from Leeds Electron Microscopy and Spectroscopy Centre (LEMAS), University of Leeds.

REFERENCES

(1) Dresselhaus, M. S.; Thomas, I. L. Alternative Energy Technologies. *Nature* **2001**, *414*, 332-337.

(2) He, J. Y.; Zou, Y. Q.; Wang, S. Y. Defect Engineering on Electrocatalysts for Gas-Evolving Reactions. *Dalton Trans.* **2019**, *48*, 15-20.

(3) Morales-Guio, C. G.; Stern, L. A.; Hu, X. Nanostructured Hydrotreating Catalysts for Electrochemical Hydrogen Evolution. *Chem. Soc. Rev.* **2014***, 43*, 6555-6569.

(4) Hou, Y.; Qiu, M.; Zhang, T.; Zhuang, X. D.; Kim, C. S.; Yuan, C.; Feng, X. L. Ternary Porous Cobalt Phosphoselenide Nanosheets: An Efficient Electrocatalyst for Electrocatalytic and Photoelectrochemical Water Splitting. *Adv. Mater.* **2017**, *29*, 1701589.

(5) Hou, Y.; Qiu, M.; Nam, G.; Kim, M. G.; Zhang, T.; Liu, K. J.; Zhuang, X. D.; Cho, J.; Yuan, C.; Feng, X. L. Integrated Hierarchical Cobalt Sulfide/Nickel Selenide Hybrid Nanosheets as an Efficient Three-dimensional Electrode for Electrochemical and Photoelectrochemical Water Splitting. *Nano Lett.* **2017**, *17*, 4202-4209.

(6) Yang, J.; Lei, C. J.; Wang, H. Q.; Yang, B.; Li, Z. J.; Qiu, M.; Zhuang, X. D.; Yuan, C.; Lei, L. C.; Hou, Y.; Feng, X. L. High-index Faceted Binary-Metal Selenide Nanosheet Arrays as Efficient 3D Electrodes for Alkaline Hydrogen Evolution. *Nanoscale* **2019**, *11*, 17571-17578.

(7) Hu, J.; Huang, B. L.; Zhang, C. X.; Wang, Z. L.; An, Y. M.; Zhou, D.; Lin, H.; Leung, M. K. H.; Yang, S. H. Engineering Stepped Edge Surface Structures of MoS_2 Sheet Stacks to Accelerate the Hydrogen Evolution Reaction. *Energy Environ. Sci.* **2017**, *10*, 593-603.

(8) Hou, Y.; Zhuang, X. D.; Feng, X. L. Recent Advances in Earth-Abundant Heterogeneous Electrocatalysts for Photoelectrochemical Water Splitting. *Small Methods* **2017**, *1*, 1700090.

(9) Gao, Q. S.; Zhang, W. B.; Shi, Z. P.; Yang, L. C.; Tang, Y. Structural Design and Electronic Modulation of Transition-metal-carbide Electrocatalysts toward Efficient Hydrogen Evolution. *Adv. Mater.* **2019**, *31*, 1802880.

(10) Xiao, P.; Sk, M. A.; Thia, L.; Ge, X. M.; Lim, R. J.; Wang, J. Y.; Lim, K. H.; Wang, X. Molybdenum Phosphide as an Efficient Electrocatalyst for the Hydrogen Evolution Reaction. *Energy Environ. Sci.* **2014**, *7*, 2624-2629.

(11) Hu, E. L.; Feng, Y. F.; Nai, J. W.; Zhao, D.; Hu, Y.; Lou, David. X.W. Construction of Hierarchical Ni-Co-P Hollow Nanobricks with Oriented Nanosheets for Efficient Overall Water Splitting. *Energy Environ. Sci.* **2018**, *11*, 872-880.

(12) Dou, S.; Wang, X.; Wang, S. Y. Rational Design of Transition Metal-Based Materials for Highly Efficient Electrocatalysis, *Small Methods* **2019**, *3*, 1800211.

(13) Zhu, Y. P.; Chen, G.; Zhong, Y. J.; Zhou, W.; Shao, Z.P. Rationally Designed Hierarchically Structured Tungsten Nitride and Nitrogen-rich Graphene-like Carbon Nanocomposite as Efficient Hydrogen Evolution Electrocatalyst. *Adv. Sci.* **2018**, *5*, 1700603.

(14) Yan, D. F.; Chen, R.; Xiao, Z. H.; Wang, S. Y. Engineering the Electronic Structure of Co_3O_4 by Carbon-Doping for Efficient overall Water Splitting. *Electrochim. Acta* **2019**, *303*, 316-322.

(15) Hu, J.; Zhang, C. X.; Jiang, L.; Lin, H.; An, Y. M.; Zhou, D.; Leung, M. K. H.; Yang, S. H. Nanohybridization of MoS_2 with Layered Double Hydroxides Efficiently Synergizes the Hydrogen Evolution in Alkaline Media. *Joule* **2017,** *1*,383-393.

(16) Geng, X. M.; Sun, W. W.; Wu, W.; Chen, B.; Al-Hilo, A.; Benamara, M.; Zhu, H. L.; Watanabe, F.; Cui, J. B.; Chen, T. P. Pure and Stable Metallic Phase Molybdenum Disulfide Nanosheets for Hydrogen Evolution Reaction. *Nat. Commun.* **2016**, *7*, 10672.

(17) Morales-Guio, C. G.; Hu, X. L. Amorphous Molybdenum Sulfides as Hydrogen Evolution Catalysts. *Acc. Chem. Res.* **2014**, *47*, 2671-2681.

(18) Jaramillo, T. F.; Jørgensen, K. P.; Bonde, J.; Nielsen, J. H.; Horch, S.; Chorkendorff, I. Identification of Active Edge Sites for Electrochemical H_2 Evolution from MoS_2 Nanocatalysts. *Science* **2007**, *317*(*6*), 100-102.

(19) Si, J.; Zheng, Q.; Chen, H.; Lei, C.; Suo, Y.; Yang, B.; Zhang, Z.; Li, Z.; Lei, L.; Hou, Y.; Ostrikov, K. Scalable Production of Few-Layer Niobium Disulfide Nanosheets via Electrochemical Exfoliation for Energy-Efficient Hydrogen Evolution Reaction. *ACS Appl. Mater. Interfaces* **2019**, *11*, 13205-13213.

(20) Sarma, P. V.; Tiwary, C. S.; Radhakrishnan, S.; Ajayan, P. M.; Shaijumon, M. M. Oxygen Incorporated WS_2 Nanoclusters with Superior Electrocatalytic Properties for Hydrogen Evolution Reaction. *Nanoscale* **2018,** *10*, 9516-9524.

(21) Kong, D. S.; Wang, H. T.; Cha, J. J.; Pasta, M.; Koski, K. J.; Yao, J.; Cui, Y. Synthesis of MoS_2 and $MoSe_2$ Flms with Vertically Aligned Layers. *Nano Lett.* **2013**, *133*, 1341-1347.

(22) Tang, H.; Dou, K. P.; Kaun, C. C.; Kuang, Q.; Yang, S. H. $MoSe_2$ Nanosheets and Their Graphene Hybrids: Synthesis, Characterization and Hydrogen Evolution Reaction Studies. *J. Mater. Chem. A* **2014**, *2*, 360-364.

(23) Tsai, C.; Chan, K.; Abild-Pedersen, F.; Nørskov, J. K. Active Edge Sites in $MoSe_2$ and WSe_2 Catalysts for the Hydrogen Evolution Reaction: A Density Functional Study. *Phys. Chem. Chem. Phys.* **2014**, *16*, 13156.

(24) Shu, H. B.; Zhou, D.; Li, F.; Cao, D.; Chen, X. S. Defect Engineering in $MoSe_2$ for the Hydrogen Evolution Reaction: From Point Defects to Edges. *ACS Appl. Mater. Interfaces* **2017**, *9*, 42688.

(25) Yu, X. Y.; Prévot, M. S.; Guijarro, N.; Sivula, K. Self-Assembled 2D WSe_2 Thin Films for Photoelectrochemical Hydrogen Production. *Nat. Commun.* **2015**, *6*, 7596.

(26) Seok, J. B.; Lee, J. H.; Cho, S. Y.; Ji, B. D.; Kim, H. W.; Kwon, M.; Kim, D. Y.; Kim, Y.M.; Oh, S. H.; Kim, S. W.; Lee, Y. H.; Son, Y. W.; Yang, H. J. Active Hydrogen Evolution through Lattice Distortion in Metallic $MoTe_2$. *2D Mater.* **2017**, *4*, 025061.

(27) Kibsgaard, J.; Chen, Z.; Reinecke, B. N.; Jaramillo, T. F. Engineering the Surface Structure of MoS_2 to Preferentially Expose Active Edge Sites for Electrocatalysis. *Nat. Mater.* **2012**, *11*, 963-969.

(28) Sun, Y.; Alimohammadi, F.; Zhang, D.; Guo, G. Enabling Colloidal Synthesis of Edge-Oriented MoS_2 with Expanded Interlayer Spacing for Enhanced HER Catalysis. *Nano Lett.* **2017**, *17*, 1963-1969.

(29) Li, X. H.; Guo, S. H.; Li, W.; Ren, X. G.; Su, J.; Song, Q.; JorgeSobrido, A.; Wei, B. Q. Edge-rich MoS_2 Grown on Edge-Oriented Three-Dimensional Graphene Glass for High-Performance Hydrogen Evolution. *Nano Energy* **2019**, *57*, 388-397.

(30) Najafi, L.; Bellani, S.; Martín-García, B.; Oropesa-Nuñez, R.; Castillo, A. E. D. R.; Prato, M.; Moreel, I.; Bonaccorso, F. Solution-Processed Hybrid Graphene Flake/2H-MoS_2 Quantum Dot Heterostructures for Efficient Electrochemical Hydrogen Evolution. *Chem. Mater.* **2017**, *29*, 5782-5786.

(31) Wu, W.; Niu, C.; Wei, C.; Jia, Y.; Li, C.; Xu, Q. Activation of MoS_2 Basal Planes for Hydrogen Evolution by Zinc. *Angew. Chem. Int. Ed.* **2019**, *58*, 2029-2033.

(32) Yu, Y. F.; Huang, S. Y.; Li, Y. P.; Steinmann, S. N.; Yang, W. T.; Cao, L. Y. Lay-Dependent Electrocatalysis of MoS_2 for Hydrogen Evolution. *Nano Lett.* **2014**, *14*, 553-558.

(33) Canton-Vitoria, R.; Sayed-Ahmad-Baraza, Y.; Pelaez-Fernandez, M.; Arenal, R.; Bittencourt, C.; Ewels, C. P.; Tagmatarchis, N.; Functionalization of MoS_2 with 1,2-Dithiolanes: Toward Donor-Acceptor Nanohybrids for Energy Conversion. *npj 2D Mater. Appl.* **2017,** *1*, 13.

(34) Wang, H. T.; Zhang, Q. F.; Yao, H. B.; Liang, Z.; Lee, H. W.; Hsu, P. C.; Zheng, G. Y.; Cui, Y. High Electrochemical Selectivity of Edge versus Terrace Sites in Two-Dimensional Layered MoS_2 Materials. *Nano Lett.* **2014**, *14*, 7138-7144.

(35) Rajendran, S.; Naushad, M.; Balakumar**,** S.; Nanostructured Materials for Energy Related Applications, ISBN: 978-3-030-04500-5.

(36) Voiry, D.; Salehi, M.; Silva, R.; Fujita, T.; Chen, M.; Asefa, T.; Shenoy, V. B.; Eda, G.; Chhowalla, M. Conducting MoS_2 Nanosheets as Catalysts for Hydrogen Evolution Reaction. *Nano Lett.* **2013**, *13*, 6222-6227.

(37) Maitra, U.; Gupta, U.; De, M.; Datta, R.; Govindaraj, A.; Rao, C. N. R. Highly Effective Visible-Light-Induced H_2 Generation by Single-Layer 1T-MoS_2 and a Nanocomposite of Few-Layer 2H-MoS_2 with Heavily Nitrogenated Graphene. *Angew. Chem. Int. Ed.* **2013**, *52*, 13057-13061.

(38) Huang, Y. H.; Sun, Y. H.; Zheng, X. L.; Aoki, T.; Pattengale, B.; Huang, J. E.; He, X.; Bian, W.; Younan, S.; Williams, N.; Hu, J.; Ge, J. X.; Pu, N.; Yan, X.;X.; Pan, X. Q.; Zhang, L. J.; Wei, Y. G.; Gu, J. Atomically Engineering Activation Sites onto Metallic 1T-MoS_2 Catalysts for Enhanced Electrochemical Hydrogen Evolution. *Nat. Commun.* **2019**, *10*(*1*), 982.

(39) Liu, Z. Q.; Li, N.; Su, C.; Zhao, H. Y.; Xu, L.L.; Yin, Z. Y.; Li, J.; Du, Y. P. Colloidal Synthesis of 1T' Phase Dominated WS_2 towards Endurable Electrocatalysis. *Nano Energy* **2018**, *50*, 176-181.

(40) Li, G. Q.; Zhang, D.; Qiao, Q.; Yu, Y. F.; Peterson, D.; Zafar, A.; Kumar, R.; Curtarolo, S.; Hunte, F.; Shannon, S.; Zhu, Y. M.; Yang, W. T.; Cao, L. Y. All the Catalytic Active Sites of MoS_2 for Hydrogen Evolution. *J. Am. Chem. Soc.* **2016,** *138*, 16632-16638.

(41) McAteer, D.; Gholamvand, Z.; McEvoy, N.; Harvey, A.; OMalley, E.; Duesberg, G. S.; Coleman, J. N. Thickness Dependence and Percolation Scaling of Hydrogen Production Rate in MoS_2 Nanosheet and Nanosheet-Carbon Nanotube Composite Catalytic Electrodes. *ACS Nano* **2016**, *10*, 672-683.

(42) Murthy, A. P.; Theerthagiri, J.; Madhavan, J.; Murugan, K. Highly Active MoS_2/Carbon Electrocatalysts for the Hydrogen Evolution Reaction-Insight into the Effect of the Internal Resistance and Roughness Factor on the Tafel Slope. *Phys. Chem. Chem. Phys.* **2017**, *19*, 1988-1998.

(43) Rowley-Neale, S. J.; Brownson, D. A. C.; Smith, G. C.; Sawtell, D. A. G.; Kelly, P.J.; Banks, C.E. 2D Nanosheet Molybdenum Disulphide (MoS_2) Modified Electrodes Explored towards the Hydrogen Evolution Reaction. *Nanoscale* **2015**, *7*, 18152-18168.

(44) Xia, Y.; Mathis, T. S.; Zhao, M. Q.; Anasori, B.; Dang, A. L.; Zhou, Z. H.; Cho, H. S.; Gogotsi, Y.; Yang, S. Thickness-Independent Capacitance of Vertically Aligned Liquid-Crystalline Mxenes, *Nature* **2018**, *557*, 409-412.

(45) Billaud, J.; Bouville, F.; Magrini, T.; Villevieille, C.; Studart, A. R. Magnetically Aligned Graphite Electrodes for High-Rate Performance Li-Ion Batteries. *Nat. Energy* **2016**, *1*, 16097.

(46) Zhang, X.; Zhang, Y.; Yu, B. B.; Yin, X. L.; Jiang, W. J.; Jiang, Y. J.; Hu, S.; Wan, L. J. Physical Vapor Deposition of Amorphous MoS_2 Nanosheet Arrays on Carbon Cloth for Highly Reproducible Large-Area Electrocatalysts for the Hydrogen Evolution Reaction. *J. Mater. Chem. A* **2015***, 3*, 19277-19281.

(47) Gao, B.; Du, X.Y.; Ma, Y. M.; Li, Y. X.; Li, Y. H.; Ding, S. J.; Song, Z. X.; Xiao, C. H. 3D Flower-Like Defected MoS_2 Magnetron-Sputtered on Candle Soot for Enhanced Hydrogen Evolution Reaction. *Appl. Catal. B-Environ* 2019, DOI: 10.1016/j.apcatb.2019.117750.

(48) Li, H.; Wu, H. Q.; Yuan, S. G.; Qian, H. Synthesis and Characterization of Vertically Standing MoS_2 Nanosheets. *Sci. Rep.* **2016**, *6*, 21171.

(49) Yu, Y. F.; Nam, G. H.; He, Q. Y.; Wu, X. J.; Zhang, K.; Yang, Z.Z.; Chen, J. Z.; Ma, Q. L.; Zhao, M.T.; Liu, Z.Q.; Ran, F. R.; Wang, X. Z.; Li, H; .Huang, X.; Li, B.; Xiong, Q. H.; Zhang, Q.; Liu, Z.; Gu, L.; Du, Y. H.; Huang, W.; Zhang, H. High Phase-Purity 1T′-MoS_2- and 1T′-$MoSe_2$-Layered Crystals. *Nature Chemistry* **2018**, *10*, 638-643.

(50) Ghim, D.; Jiang, Q. S.; Cao, S. S.; Singamaneni, S.; Jun, Y. S. Mechanically Interlocked 1T/2H Phases of MoS_2 Nanosheets for Solar Thermal Water Purification. *Nano Energy* **2018**, *53*, 949-957.

(51) Hakala, M.; Kronberg, R.; Laasonen, K. Hydrogen Adsorption on Doped MoS_2 Nanostructures *Sci. Rep.* **2017**, *7*, 15243.

(52) Kronberg, R.; Hakala, M.; Holmberg, N.; Laasonen, K. Hydrogen Adsorption on MoS_2-Surfaces: A DFT Study on Preferential Sites and the Effect of Sulfur and Hydrogen Coverage. *Phys. Chem. Chem. Phys.* **2017**, *19*, 16231-16241.

(53) Grønborg, S. S.; Salazar, N.; Bruix, A.; Rodríguez-Fernández, J.; Thomsen, S. D.; Hammer, B.; Lauritsen, J. V. Visualizing Hydrogen-Induced Reshaping and Edge Activation in MoS_2 and Co-Promoted MoS_2 Catalyst Clusters. *Nat. Commun.* **2018**, *9*, 2211.

(54) Asadi1, M.; Kumar, B.; Behranginia, A.; Rosen, B. A.; Baskin, A.; Repnin, N.; Pisasale, D.; Phillips, P.; Zhu, W.; Haasch, R.; Klie, R. F.; Král, P.; Abiade, J.; Salehi-Khojin, A. Robust Carbon Dioxide Reduction on Molybdenum Disulphide Edges. *Nat. Commun.* **2014**, *5*, 4470.

(55) Thornton, J. A. Influence of Apparatus Geometry and Deposition Conditions on the Structure and Topography of Thick Sputtered Coatings. *J. Vac. Sci. Technol.* **1974**, *11*(*4*), 666-670.

(56) Kluth, O.; Schöpe, G.; Hüpkes, J.; Agashe, C.; Müller, J.; Rech, B. Modified Thornton Model for Magnetron Sputtered Zinc Oxide: Film Structure and Etching Behaviour. *Thin Solid Films* **2003**, *442*, 80-85.

(57) Spalvins, T. Frictional and Morphological Properties of Au-MoS_2 Films Sputtered from a Compact Target. *Thin Solid Films* **1984**, *118*, 375-384.

(58) Xu, S. S.; Gao, X. M.; Hu, M.; Sun, J. Y.; Jiang, D.; Zhou, F.; Liu, W. M.; Weng, L. J. Nanostructured WS_2-Ni Composite Films for Improved Oxidation, Resistance and Tribological Performance. *Appl. Surf. Sci.* **2014**, *288*, 15-25.

(59) Weiss, K.; Phillips, J. M. Calculated Specific Surface Energy of Molybdenite (MoS_2). *Phys. Rev. B* **1976**, *14*, 5392.

(60) Muratore, C.; Hu, J. J.; Wang, B.; Haque, M. A.; Bultman, J. E.; Jespersen, M. L.; Shamberger, P. J.; McConney, M. E.; Naguy, R. D.; Voevodin, A. A. Continuous Ultra-Thin MoS_2 Films Grown by Low-Temperature Physical Vapour Deposition. *Appl. Phys. Lett.* **2014**, *104*, 261604.

(61) Geim, A. K.; Grigorieva, I. V. Van Der Waals Heterostructures. *Nature* **2013**, *499*, 419-425.

(62) Spirko, J. A.; Neiman, M. L.; Oelker, A. M.; Klier K. Electronic Structure and Reactivity of Defect MoS_2: I. Relative Stabilities of Clusters and Edges, and Electronic Surface States. *Surf. Sci.* **2003**, *542*, 192-204.

(63) Kumar, P.; Viswanath, B. Horizontally and Vertically Aligned Growth of Strained MoS_2 Layers with Dissimilar Wetting and Catalytic Behaviors. *CrystEngComm* **2017**, *19*, 5068-5078.

(64) Conway, B. E.; Tilak, B. V. Interfacial Processes Involving Electrocatalytic Evolution and Oxidation of H_2, and the Role of Chemisorbed H. *Electrochim. Acta* **2002**, *47*, 3571-3594.

(65) Voiry, D.; Yang, J. U.; Chhowalla, M. Recent Strategies for Improving the Catalytic Activity of 2D TMD Nanosheets toward the Hydrogen Evolution Reaction. *Adv. Mater.* **2016**, *28*, 6197-6206.

(66) McCrory, C. C.;L.; Jung, S.; Ferrer, I. M.; Chatman, S. M.; Peters, J. C.; Jaramillo, T. F.; Benchmarking Hydrogen Evolving Reaction and Oxygen Evolving Reaction Electrocatalysts for Solar Water Splitting Devices. *J. Am. Chem. Soc.* **2015**, *137*, 4347-4357.

(67) Cunningham, G.; Khan, U.; Backes, C.; Hanlon, D.; McCloskey, D.; Donegan, J. F.; Coleman, J. N. Photoconductivity of Solution-Processed MoS_2 Films. *J. Mater. Chem. C* **2013**, *1*, 6899-6904.

(68) Cunningham, G.; Hanlon, D.; McEvoy, N.; Duesberg, G. S.; Coleman, J. N. Large Variations in both Dark- and Photoconductivity in Nanosheet Networks as Nanomaterial is Varied from MoS_2 to WTe_2. *Nanoscale* **2015**, *7*, 198-208.

GRAPHICAL ABSTRACT